Effect of accelerators on $Ca(OH)_2$ activated ground granulated blast-furnace slag at low curing temperature

Qi Zhai [a], Kiyofumi Kurumisawa [b, *]

[a] Division of Sustainable Resources Engineering, Graduate School of Engineering, Hokkaido University, Japan

[b] Division of Sustainable Resources Engineering, Faculty of Engineering, Hokkaido University, Japan

Abstract

The early effects of three accelerators on a $Ca(OH)_2$ activated ground granulated blast-furnace slag binder at low curing temperatures are discussed. The compressive strength, hydration kinetics, hydration products, and microstructures were investigated by isothermal calorimetry, X-ray diffraction, mercury intrusion porosimetry, scanning electron microscopy, and nuclear magnetic resonance. Results show that accelerators continue to promote the strength development of pastes in the early stage during low-temperature curing, especially with sodium sulfate, which exhibits a higher strength and hydration degree in the early stage. However, accelerators cannot effectively improve the pore structure at low-temperature curing, which severely restricts the development of strength, compared with that at 20 °C. Furthermore, a good correlation was found between the initial strength development and the limit equivalent ionic conductivity (LEIC), suggesting that LEIC influences the reaction acceleration of blast-furnace slag at an early age.

Keywords: GGBFS, Additives, low curing temperature, MIP, BSE, LEIC

1. Introduction

Ordinary Portland cement (OPC) has a long history of almost 200 years as a widely used building material. Within the recent years facing increasing production of OPC, a series of problems have arisen. For cement production, raw materials must be heated to 1450 °C, which not only consumes a considerable amount of energy, but as the raw materials are calcined, a large amount of carbon dioxide is emitted, causing severe environmental pollution [1]. Presently, an increasing number of researchers are studying the properties of green cementitious materials, such as ground granulated blast-furnace slag (GGBFS) and fly ash (FA), which are called supplementary cementitious materials (SCMs) to replace part of the cement to make composite cement [2–4]. The use of composite cement not only effectively reduces carbon dioxide emissions, but also improves durability and thermal and mechanical properties [5–7].
Blast-furnace slag is widely used as one of many SCMs. It is a by-product produced by a high-temperature reaction between the flux and iron ore when the temperature of the

blast furnace reaches 1350–1550 °C, which contains more than 95% glass phase and has potential hydraulic properties [1]. Numerous researchers have addressed the hydration performance of blast furnace slag cement (BFSC) and revealed the low early strength of BFSC and strong later age compressive strength [8–10]. This may affect the construction period in cold regions with higher latitudes and severely restrict the use of blast-furnace slag. Therefore, effort has been devoted to improving the early strength of BFSCs. Ben-dor et al. [11] studied the effects of calcium chloride ($CaCl_2$), chromium chloride ($CrCl_3$), and cadmium iodide (CdI_2) on the strength of Portland cement and combined these effects with the morphology of C-S-H. CdI_2 reported that thee morphology of the corresponding C-S-H was "sponge-like," $CrCl_3$ and $CaCl_2$ promoted the hydration of cement, and the morphology of C-S-H was a "honeycomb". Kondo et al. [12] studied the influence of lime, lime + gypsum, and sodium hydroxide (NaOH) on the hydration of super-sulfated slag cement, and revealed that too little lime or Portland cement (PC) would lead to a smaller slag reaction quantity and a smaller reaction rate with too much addition. Vehams et al. [13] observed a synergistic effect between $CaCl_2$, lime, and quartz fillers. $CaCl_2$ promoted the hydration of cement during the early age stage. The filler provided more space for the nodules of the hydration products and promoted cement hydration during the acceleration stage. Bellmann et al. [8] attempted to improve the early strength by activating blast furnace slag using different types of salts. Myrdal et al. [14] and Tao et al. [15] described in detail the types of cement accelerators and the mechanism of hydration. According to different purposes, cement accelerators can be classified according to the following standards, according to which the effect can be divided into promoting setting or hardening. Aggoun et al. [16] confirmed the promoting effect of calcium nitrate ($Ca(NO_3)_2$), triethanolamine (TEA), and triesopropanolamine (TIPA) using a calorimeter test. They concluded that $Ca(NO_3)_2$ mainly promoted the setting time of cement slurry, while TEA and TIPA mainly promoted the hardening of cement slurry, and $Ca(NO_3)_2$ combined with them accelerated the setting and enhanced the hardening. Riding et al. [17] studied the hydration promoting effect of diethanol-isopropanolamine (DEIPA) and $CaCl_2$ on cement and cement slag mixtures and concluded that DEIPA reduced and changed the morphology of Portlandite, which may lead to an increase in the calcium-to-silica ratio in the C-S-H gel. According to the composition can be divided into inorganic or organic salts. Usually, researchers classify them according to their chemical composition. Some accelerators affect the hydration of tricalcium silicate (C_3A) by promoting the dissolution of silica and alumina and interfering with the influence of gypsum on tricalcium aluminate, thereby affecting the setting time. Myrdal et al. [14] explained that the promotion mechanism of $Ca(NO_3)_2$ is that the addition of $Ca(NO_3)_2$ can reduce the concentration of sulfate and the production of ettringite, thus shortening the hydration time of C_3A. There are some accelerators that may affect the tricalcium silicate phase and the formation of C-S-H gel. Tao et al. [15] revealed that calcium salts increase the concentration of calcium ions, facilitating the supersaturation of calcium hydroxide. Therefore, the initial crystallization and renewal time of tricalcium silicate hydration are shortened. Some accelerators, such as $CaCl_2$, Ca $(NO_3)_2$, and calcium formate (Ca $(HCOO)_2$), simultaneously promote setting and hardening at the same time.

Compared with inorganic salts such as calcium chloride, the use of organic salts can lessen the problem of corrosion of steel bars in reinforced concrete. The role of organic salts is more complicated than that of inorganic salts; however, Bellmann et al. pointed out that the effect of organic salts is weaker than that of inorganic salts, which may be related to the size of the anion [8]. The smaller the anion of the accelerator, the easier it is to penetrate the structure of C-S-H condensation, thereby accelerating the hydration of the unhydrated part. Kondo et al. [18] discussed the relationship between the limit equivalent ionic conductivity (LEIC) of inorganic salt anions (equivalent to the mobility) and the promotion of tricalcium silicate hydration, and showed that in addition to calcium salt, the most insoluble inorganic salt had the largest retarding effect. Furthermore, the solubility of accelerators also has a significant impact on their promotion. It is difficult for insoluble accelerators to affect the hydration of the cement. Fu et al. [19] revealed a possible reason that sodium sulfate (Na_2SO_4) promoted the dissolution of slag in slag cement from the perspective of pore solution chemistry. On the one hand, the addition of Na_2SO_4 enhanced the ionic strength of the solution, while on the other hand, the sulfate ion reacted with calcium ion to form gypsum, which promoted the formation of ettringite and reduced the activity of calcium ion, resulting in slag undersaturation. In addition, with an increase in the pH, the hydrolysis of Si-O was accelerated. The dissolution of slag provided more aluminum ions and promoted the formation of ettringite.

Because the proportion of the chemical composition of slag is slightly different from that of cement, its hydration mechanism is likewise different. The glass phase of the slag has a phase separation structure, which is divided into a continuous calcium-rich phase and a discontinuous silicon-rich phase. The calcium-rich phase accounts for the majority of the slag and is wrapped with a silicon-rich phase, which is the central structure of slag. When water is mixed with slag powder without an accelerator, a small amount of calcium ions is released into the solution to form a calcium-deficient aluminate protective film on the surface of the slag. Therefore, when the slag meets the strong alkali solution, the protective film on the slag surface is first broken and enters deep into the silicon-rich phase, which causes the Si-O-Si, Si-O-Al, and other covalent bonds to break, such that the glass phase of the slag disintegrates and recombines to produce new hydration products [20]. Richardson et al. [21] used a thermodynamic model, SEM, TGA, and other methods to estimate the stoichiometry of the hydration reaction of slag and calcium hydroxide system and revealed that the Ca/Si ratio of the C-S-H gel in the system was low, at approximately 1.35. According to Richardson's research, Biernacki et al. [22] calculated the hydration kinetics of slag / CH system based on Knudsen's kinetic model, and obtained the activation energy of slag / CH system from 14 to 22 kJ / (g·mol). Ojima et al. [23] studied the mechanism of the effect of the new accelerator on the early strength of BFSCs and revealed that the hydration rate of cement is proportional to the ultimate equivalent electrical conductivity of anions in the accelerator. Yamada et al. [24] studied the influence mechanism of accelerators on the early strength of blast-furnace slag powder in BFSCs.

The curing temperature has been studied by numerous researchers as another very important external factor affecting cement hydration. Federowicz et al. [25] studied the

effects of steam curing and water curing at different curing temperatures on the early strength of blast-furnace slag cement mortar. Serna et al. [26] studied the effect of high-temperature curing on the early strength and pore structure of alkali-activated blast-furnace slag paste. Numerous studies revealed that high-temperature curing is helpful in improving the early strength of cement [27–30]. However, under high-temperature curing conditions, the hydration products cannot be evenly distributed owing to the crossover effect, which is not conducive to the development of long-term strength [29]. In addition, numerous cold regions, such as Hokkaido in Japan, are covered with ice and snow for half a year, and the average daily minimum temperature in the coldest month is –7 °C. In such an environment, it is unrealistic to adopt high-temperature curing at construction sites. To make cement more widely used, some researchers have studied the effects of low-temperature curing conditions on the early strength, microstructure, and other properties of cement [31–33]. Wei et al.[33] investigated the effect of low-temperature curing on the early strength and microstructure of alkali-activated composites and showed that low-temperature curing had negative effects on the pore volume, early strength, and hydration degree of the samples.

However, few researchers addressed the effect of chemical accelerators on the hydration of slag powder under low-temperature curing. To the best of our knowledge, this is the first time the mechanisms of accelerators in the early hydration of blast-furnace slag powder under low-temperature curing are discussed in depth. Based on previous research [23,24], this study investigated the effects of Na_2SO_4, $Ca(HCOO)_2$, and $Ca(NO_2)_2$ on the hydration of blast-furnace slag pastes under low-temperature curing, especially the pore structure, hydration degree, and hydration of blast-furnace slag paste, and confirmed whether these influences have an impact on the strength of slag cement mortar under the same curing environment. This study provides an important complement to the knowledge of cementitious materials based on the alkaline blast-furnace slag.

2. Experimental methods

2.1 Raw materials and mix proportions

Ground granulated blast-furnace slag (GGBFS) was provided by Nippon Steel (ST60 compliant with JIS A 6206, density of 2.89 g/cm^{3}and, and specific surface area is 6010 cm^2/g), sand was provided by the Japan Cement Association (compliant with JIS R 5201), and one source of reagent-grade $Ca(OH)_2$ (CH) was obtained from Kanto Chemical Co. Inc., and used as raw materials. Figure 1 shows the X-ray diffraction pattern of GGBFS using corundum as an internal standard. The chemical composition of the materials determined by XRF are summarized in Table 1. The accelerators used in this study included $NaSO_4$, $Ca(HCOO)_2$, and $Ca(NO_2)_2$, all of which were of analytical grade, with a dosage of 0.1 mol/1 kg.The pastes and mortars had a water-to-solids mass ratio of 0.55, a BFS to CH mass ratio of 4, and a sand-to-binder ratio of mortar of 3: 1. The mix proportions of the mortars studied are shown in Table 2. Before preparing the samples, the accelerators were fully mixed with deionized water and completely dissolved. Mortars were prepared as follows: the BFS and CH powders and sand

were added to a standard epicyclical five-liter HOBART mixer. The powders were mixed at a low velocity for 30 s, after which an accelerator was added and mixed for 90 s. The samples were homogenized using a trowel for 30 s, followed by high-speed mixing for 120 s. The specimens were cast in cylinders of 100 mm length and 50 mm in diameter and sealed with two layers of plastic wrap. Once the casting was completed, half of the specimens were immediately placed in a 5 °C constant-temperature curing chamber for curing for 3, 7, and 28 days. The other specimens were sealed and cured to a specific age at 20 °C.

The pastes were prepared as follows: the BFS and CH powders were added to a standard epicyclical two-liter HOBART mixer. The powders were at low velocity for 30 s, after which an accelerator was added and mixed for 90 s. Then, the samples were homogenized using a trowel for 30 s, followed by high-speed mixing for 120 s. Specimens for electrical resistivity measurement were cast in cylinders of a length diameter of 40 mm, and other specimens were cast in cylinders of a length and diameter of 50 mm. Half of the specimens were cured in a 5 °C constant curing chamber for 1, 3, 7, and 28 days.

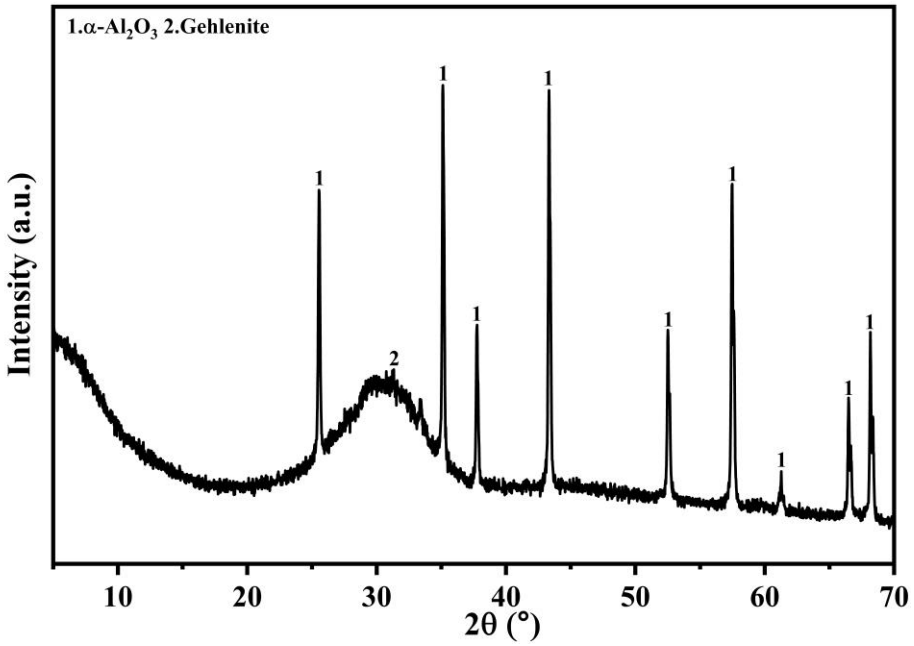

Fig. 1. XRD patterns of GGBFS

Table 1
Chemical composition of materials (mass%).

Component	BFS	Component	Sand	Component	CH
SO_3	0.7387	SiO_2	98.4	$Ca(OH)_2$	97.5
SiO_2	33.75	Al_2O_3	0.4	$CaCO_3$	1.0
TiO_2	0.517	Fe_2O_3	0.40	Cl	< 0.005
Al_2O_3	13.318	CaO	0.20	Sulfur compounds as SO_4	< 0.01
Fe_2O_3	0.664	MgO	0.00	Na	< 0.02
MnO	0.171	Na_2O	0.01	Mg	< 0.5
MgO	7.242	K_2O	0.01	Pb	< 0.001
CaO	41.793			As(ppm)	0.2

Na_2O	0.388	Fe	0.013
K_2O	0.298		
P_2O_5	0.011		

Table 2
Mix design of the mortar (g).

Mixes	BFS	Sand	CH	accelerator	Curing temperature	Water/binder ratio
Con1	760	2850	190	/	20° C	0.55
Con2				/	5° C	
NS1				13.49	20° C	
NS2				13.49	5° C	
CN1				12.35	20° C	
CN2				12.35	5° C	
CF1				14.25	20° C	
CF2				14.25	5° C	

Notes: NS=Na_2SO_4; CN=$Ca(NO_2)_2$; CF=$Ca(HCOO)_2$; CH=$Ca(OH)_2$.

2.2 Hydration stopping procedure

The solvent exchange method was used to stop the hydration of the sample for the corresponding test at a specific age. Solvent exchange is the preferred method for XRD, NMR, MIP, and SEM analyses. Most solvents can preserve chemically bound water in the hydrate phase and microstructure [34]. In this study, acetone was used as a solvent to stop the hydration of the specimens. At the appropriate age, specimens were removed from the molds, and the specimens were broken into pieces with a hammer. Fragments with a size of 2–5 mm were screened using a standard test screen. After screening, the samples were immersed in acetone for 2 h. After removal from acetone, the samples were placed in a fume hood for at least 1 h to dry the solvent on the surface. The samples were then placed in a curing chamber at 40 °C for 24 h to evaporate the acetone inside and spread the carbon dioxide absorbing materials around the samples to prevent carbonization. After drying, the samples were sealed in a vacuum bag for preparation.

2.3 Test methods

2.3.1 Compressive strength

The compressive strength measurements were carried out using a Hi-ACTIS-2000 testing machine in accordance with mortar specimens at 3, 7, and 28 days. Two specimens from each group were removed from the curing chamber at each time point for the compressive strength test. The compressive strength values were taken as the average of two specimens in each group to avoid contingency and calculated from the maximum stress divided by the area of the sample surface. The strength increase rate was calculated using the following formula:

$$Strength\ increase\ rate = \frac{strength_t - strength_3}{strength_3} \quad (1)$$

where $strength_t$ is the strength measured at a certain test day, $strength_3$ is the strength at

3d.

2.3.2 Electrical resistivity measurement

In this study, an impedance analyzer (HIOKI IM3570) was used to measure the electrical resistivity. Before preparing the specimen for measurement, the stainless electrodes with a distance of 30 mm were inserted on the cover, and the size of the stainless electrode was 30 mm × 30 mm. The electrical resistivity was measured with an applied voltage of 0.1 V, in the range of 4 Hz–5 MHz. To ensure the accuracy of the experiment, the specimens cured at different temperatures were placed in curing chambers at 5 and 20 °C until they were tested. After the test was completed, it was immediately returned to the curing chamber, and the test time of one specimen did not exceed 1 min/each time. The electrical resistivity was measured at 0, 1, 3, and 6, hours and 1, 3, 7, and 28 days after mixing. The measured electrical resistivity values were normalized by dividing the values at the time of the measurement by that at 0 h for each sample. Since the electrical resistivity changes depending on the concentration of the pore solution, in this study, normalization was performed by the electrical resistivity for 0 hours to eliminate it.

2.3.3 Mercury intrusion porosimetry (MIP)

The MIP method is widely employed to evaluate the pore size distribution and porosity of materials [37]. In this study, MIP was used to measure the pore size distribution for pores with diameters ranging from 3 nm to 400 μm (curing ages: 3, 7, and 28 days) with specimens cured at different temperatures. The effect of accelerators at low curing temperatures on the pore size distribution of the BFS/CH paste was estimated using the MIP test.

2.3.4 Isothermal conduction calorimetry

A six-channel isothermal calorimeter (MMC-5116; Tokyo Riko) was used to monitor the kinetics of paste hydration with the chemical accelerators at 5 and 20 ˚C, respectively. Before testing, the calorimeter was equilibrated to the corresponding temperature for 12 h. A total of 16 g BFS and 4 g CH were placed with 11 g of deionized water combined with 0.1 mol/1 kg accelerators in a 100 ml ampoule. After hand mixing for 5 min, the samples were placed in a calorimeter to record the heat release over seven days.

2.3.5 X-ray diffraction (XRD)

Some crushed samples were ground into powder and used for the XRD test. XRD was carried out on a MultiFlex (Rigaku Co., Ltd., Tokyo, Japan) using Cu-Kα radiation. The test parameters were set to a voltage of 40 kV, a current of 40 mA, a scan range of 5°–70° (2θ), step size of 0.02°, and scan speed of 2°/min.

2.3.6 SEM BSE image analysis

Quantitative analysis of the SEM images was performed on polished BFS paste sections. Before the test, the polished specimens were placed in a vacuum box. Before testing, the specimens were coated with platinum to increase their conductivity. The percent area (equivalent to% volume) of anhydrous BFS, portlandite, C–S–H, and porosity were quantified by automatic SEM image analysis. The calculation formula for the BFS hydration reaction (S) is as follows:

$$S = 1 - \frac{v_i}{v_0} \quad (2)$$

where v_0 is the volume fraction of BFS before the reaction, and v_i is the volume fraction of unhydrated BFS at age i.

2.3.7 NMR

Solid-state MAS-NMR spectra were recorded using an AVANCE III600WB Bruker NMR

instrument. The ^{29}Si DD MAS-NMR spectra (119.26 MHz) were collected using proton decoupling with a 90° pulse, a pulse repetition delay of 20 s, and a spinning rate of 12 kHz for quantitative analysis, as the reference material $C_6H_{18}O_3Si_3$ was used. The ^{27}Al MAS-NMR (156.4 MHz) spectra were collected with a repetition delay of 5 s and a spinning rate of 12 kHz. As the reference material, 1.0M Al $(NO_3)_3$ aqueous solution was used as the reference material.

3. Results and discussion

3.1 Compressive strength

The compressive strength and compressive strength increase rate of the mortar samples at different curing temperatures are shown in Fig. 2. For samples cured at 20 °C, the initial strength of all the samples with added accelerators was higher than that of the control group; in particular, the strength of NS was twice that of the control group when the curing age was three days. The 28-day strength of the control group was higher than that of all the samples with the accelerator. This is consistent with the trends reported by other researchers [38]. For the samples cured at 5 °C, the overall strength development was slow, and the strength of the samples cured at 20 °C was approximately twice the corresponding strength under 5 °C curing. The 28-day strength samples cured at 5 °C could barely reach the 7-day strength of samples cured at 20 °C, which may be related to the slow reaction at low temperature. However, the development trend of early strength was consistent with that cured at 20 °C. At the age of 28 days, the strength of the samples with the accelerator under low-temperature curing was still stronger than that of the control group. However, the strength of NS was the same as that under 20 °C curing, and the increase rate showed a downward trend, as shown in Fig. 2. (b). This may be due to the high strength development of NS samples in the early stage and the insufficient upper limit of strength development in the later stage. It may also be related to porosity and degree of hydration, and a previous study reported that NS can reduce the hydration rates of cement in the later stage [39], and it may be the same for BFS, which will be discussed in the following sections.

Overall, the strength test results showed that, in the low-temperature curing environment, although the strength development of the sample was relatively slow, the accelerator continued to promote the development of the early strength of the sample, and even had a certain role in promoting the strength at 28 days of age.

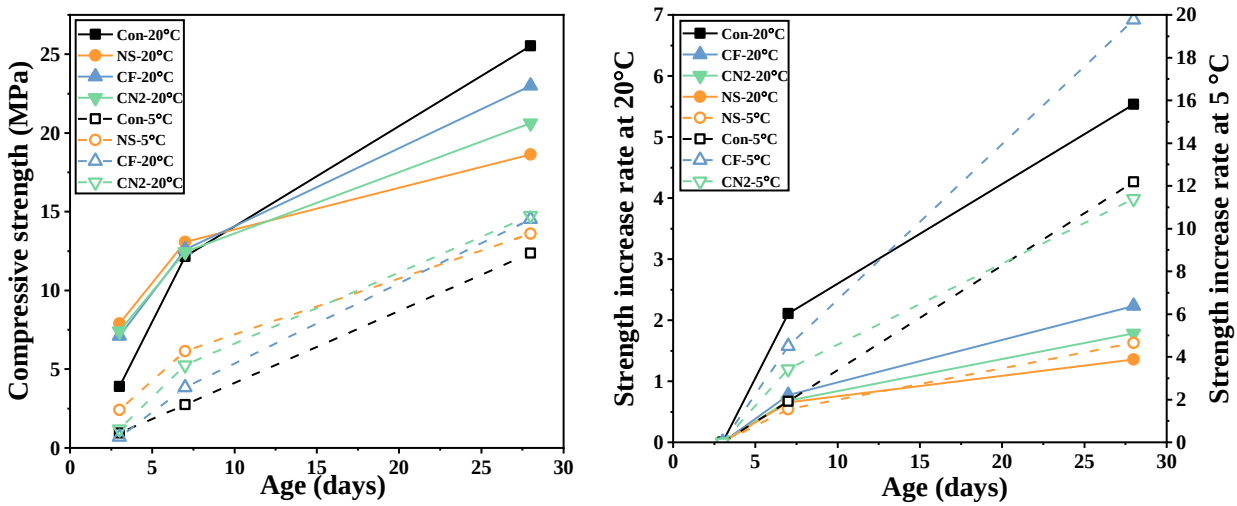

Fig. 2. Compressive strength and strength increase rate of mortar samples, with different accelerators, cured under different temperatures.

3.2 Electrical resistivity measurement

The normalized electrical resistivity results are shown in Figure 3. For the specimens cured at 20 °C, all the specimens show a downward trend in the initial stage, which indicates that the BFS starts to react upon mixing with water, and the partially dissolved ions increase the ionic strength of the pore solution, resulting in a decrease in electrical resistivity. The resistivity of NS decreased for the longest time until about the sixth hour, and the resistivity remained at a very low level. This may be because sodium sulfate increases the pH value and promotes the dissolution of slag, as shown in the following formula [19]:

$$Na_2SO_4 + Ca(OH)_2 + 2H_2O \rightarrow CaSO_4.2H_2O + 2NaOH \quad (3)$$

The resistivity of CN2 increases rapidly from 3 to 28 days, to approximately four times that of the other specimens. At the early stage, the resistivity of all the specimens with added accelerator was higher than that of the control group. On 28 day, the resistivity order from largest to smallest was CN > CF > Con > NS.

The resistivity of the specimens at a curing temperature of 5 °C exhibited a slightly different trend at an early stage. The resistivity of all specimens at an early age was stable, which was related to the lower reaction degree caused by the low temperature. Owing to the slower decomposition rate of BFS at low temperatures and the continuous production of hydration products, the resistivity tended to remain balanced and did not decrease. The later development trend of resistivity was consistent with the performance at 20 °C.

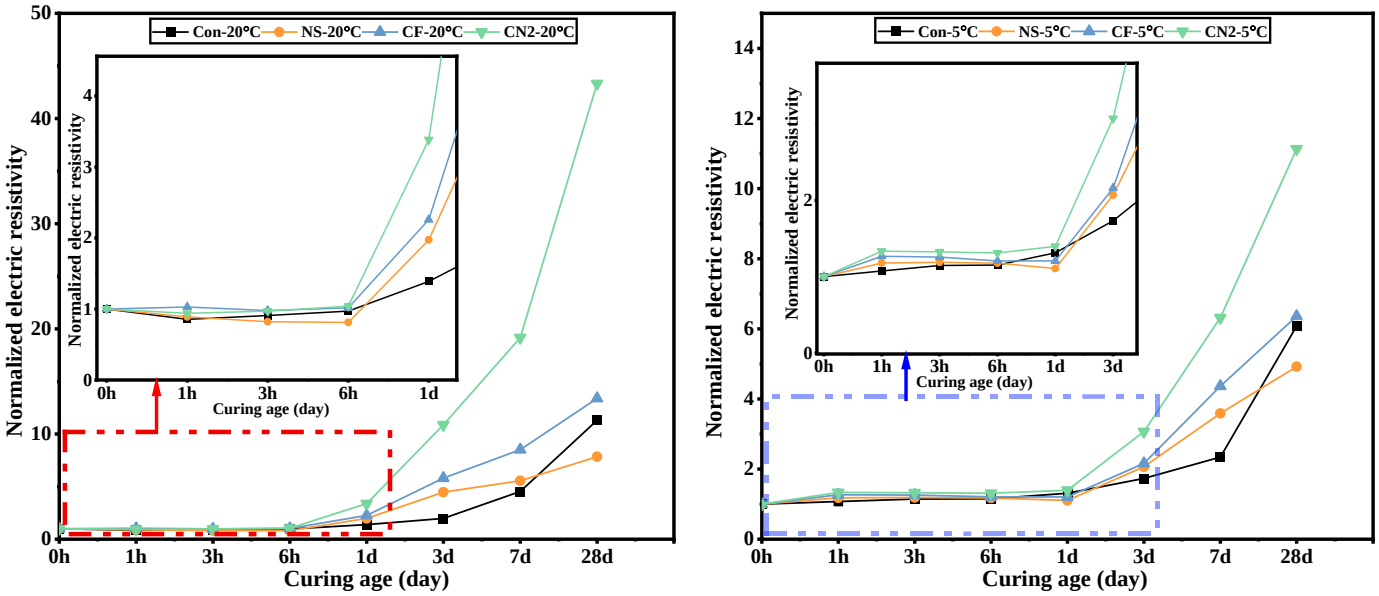

Fig. 3. Normalized electrical resistivity of specimens cured under different temperatures.

3.3 Mercury intrusion porosimetry (MIP)

MIP tests were carried out to reveal the effect of accelerators at low curing temperatures on the pore size distribution of the pastes. Fig. 4 shows the pore distribution and structure of pastes cured at 5 and 20 °C with different accelerators. The pore size distribution of the pastes cured at 20 °C is shown in Figure S1 (Supplementary Information). Fig.4 (b) and (d) show the shifts of the mercury intrusion peaks, which record the critical pore radii that appear with a high frequency [40,41]. The critical pore radii of all specimens at 3 day were mainly concentrated in the range of 1100–1300 nm. The peak value of NS was lower than that of other specimens, which might contribute to the similar hydration degrees of all samples, whereas the NS strength was slightly higher. Then, the peaks gradually shift to 24 nm at 7 days, except for NS (see Figure S2), which was related to the formation of hydration products, especially C-A-S-H, whose needle shape effectively filled the pores. The peak position of NS was approximately 47 nm, which may be related to the production of ettringite. Finally, the main peak of all specimens except NS shifted to approximately 20 nm, and the NS peak was approximately 31 nm. Notably, all specimens except NS have two peaks, which means that NS may change the pore connectivity.

Fig. 4 (a) and (c) show the pore size distributions of the pastes at different temperatures. Regardless of the curing temperature, the overall distribution trend of all specimens from 3 to 28 days was developing toward a smaller pore size. The changing trend of the pore size distribution of the specimens with accelerators under low-temperature curing and room-temperature curing were roughly the same, and the pore size distribution of most specimens in the early stage was smaller than that of the control specimens, which meant that the accelerators could improve the porosity and pore structure at low temperatures in the early stage. However, regardless of age, the pore size distribution of all specimens cured at low temperature was larger than that of samples cured at room temperature, which indicated that the accelerator could not effectively improve the porosity at low temperatures compared with that at 20 °C, which was one of the reasons for the low strength of the samples cured at low temperatures. This can be

seen more intuitively in Fig. 5.

It is defined as follows based on the magnitude of the effect on strength development and permeability,: harmless pores (< 20 nm), less harmful pores (20–50 nm), harmful pores (50–200 nm), and more harmful pores (> 200 nm) [33,40,42]. Fig. 5 shows the pore volume fraction in the cumulative porosity of each specimen at different ages. Zhang et al. [43] reported that pore sizes above 50 nm are more related to compressive strength, and pore sizes below 10 nm are related to the pore structure. As shown in Fig. 5, regardless of the curing temperature, the volume fraction of pores above 50 nm in all the specimens decreased. At a curing temperature of 20 °C, compared with the control specimen, the specimen with the accelerator had a better effect of pore refinement in the early stage. In contrast, the specimens cured at low temperature did not exhibit such characteristics, which may be related to the low reaction degree. Note that the volume fraction of pore size above 50 nm of NS under 20 °C curing, especially that of pore size above 200 nm, was significantly smaller than that of other specimens from 3 day, but remained approximately 9 % from 3 to 28 day, which was very similar to the tendency of the hydration degree of NS measured by BSE (see figure10). In contrast, the ratio of pores below 20 nm in the Con, CN2, and CF specimens at Day 28 was 30, 27, and 29 %, respectively, which was higher than that of NS, indicating that NS could not play an effective role in the refinement of the pore structure, although the porosity of NS was the lowest at all hydration stages.

From the data of specimens cured at 5 °C, it seems that the accelerator could not improve the pore structure effectively under low-temperature curing, but it could reduce the porosity to some extent.

Figure 6 shows the relationship between compressive strength and capillary porosity. At the early stage, compressive strength was associated with capillary porosity; the smaller the porosity, the greater the strength. However, when the age increased to 28 days, the total porosity reduction of all specimens was very low, approximately 2 %. As shown in Fig. 4, the peak value of the pore size shifted to about 20 nm. This indicates that the C-A-S-H produced was only refined enough, but could not fill pores, especially for the specimen with accelerators, which may be related to the accelerators changing the morphology of C-A-S-H.

Analyzed together, at low-temperature curing, compared with the control group, although the accelerator could reduce the porosity to a certain extent, it could not effectively improve the pore structure. In the early stage of hydration, there was a good relationship between the porosity and compressive strength of the specimen. In the later stage, even if the accelerator could further reduce the porosity, it could not reduce the ratio of harmful pores, which may also be one of the factors hindering the further development of strength.

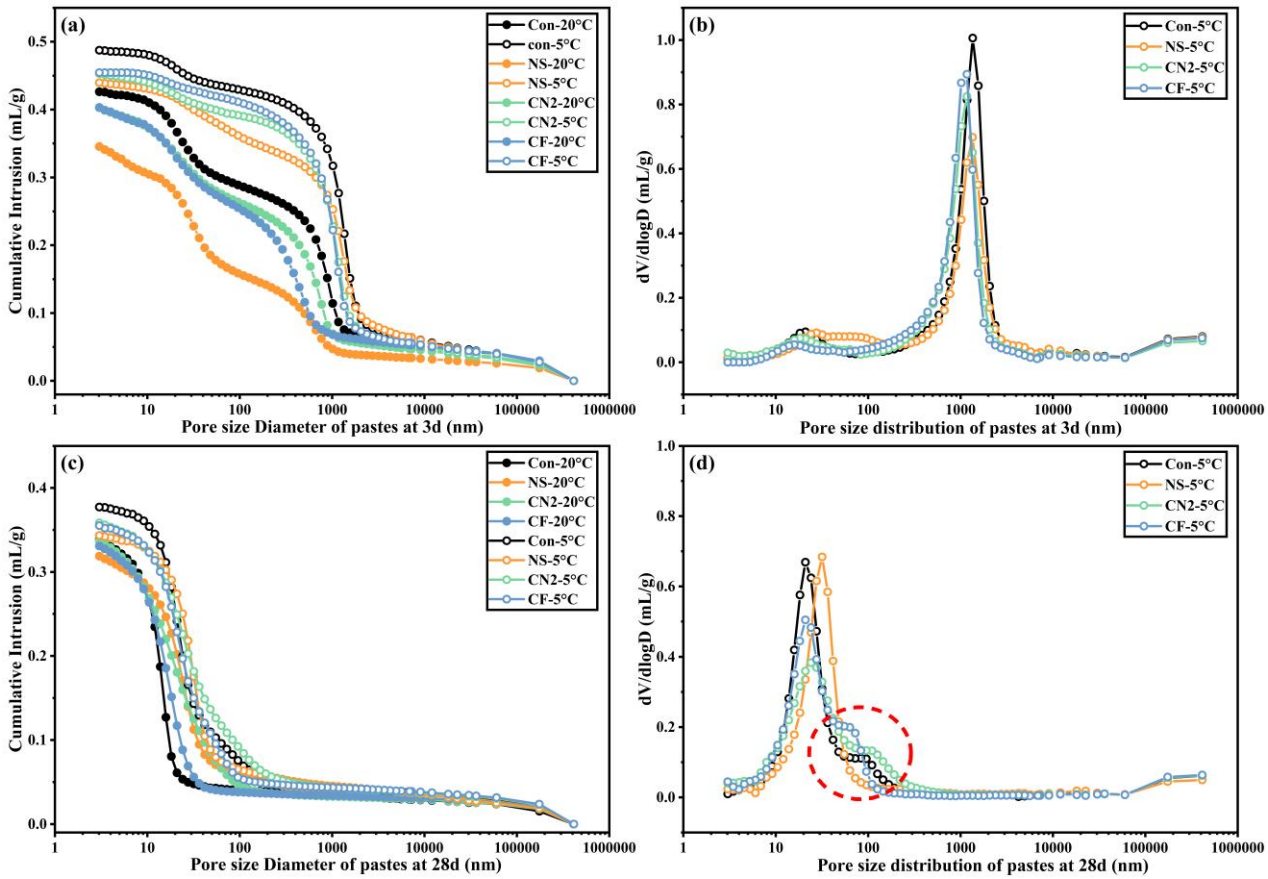

Fig. 4. Pore size distribution of pastes.

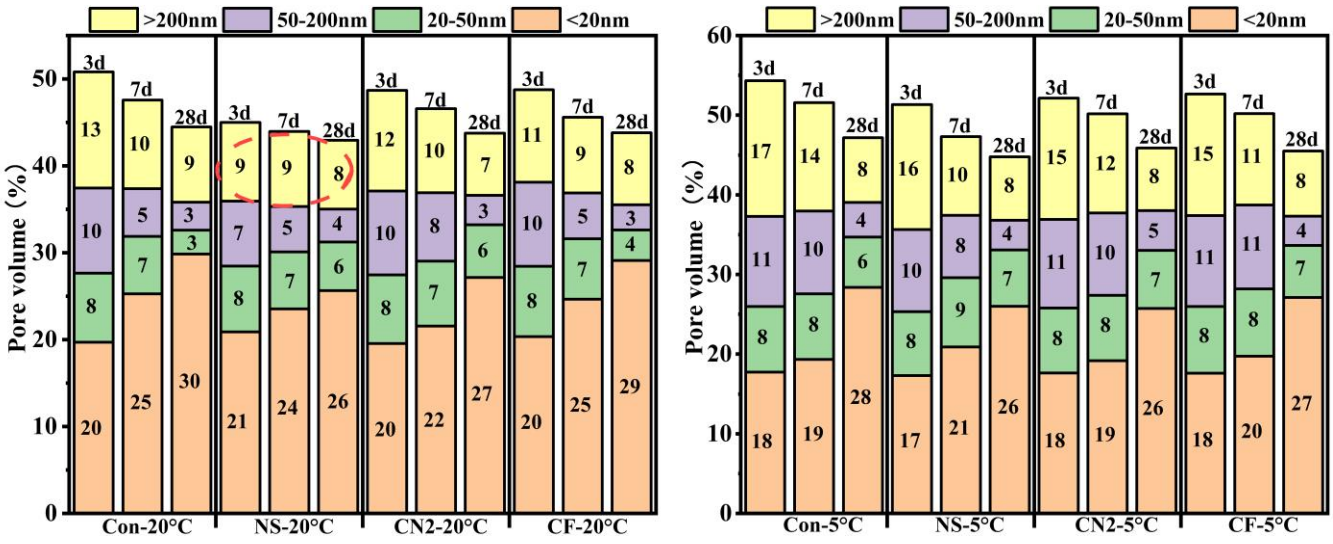

Fig. 5. Pore volume of samples at different curing temperatures

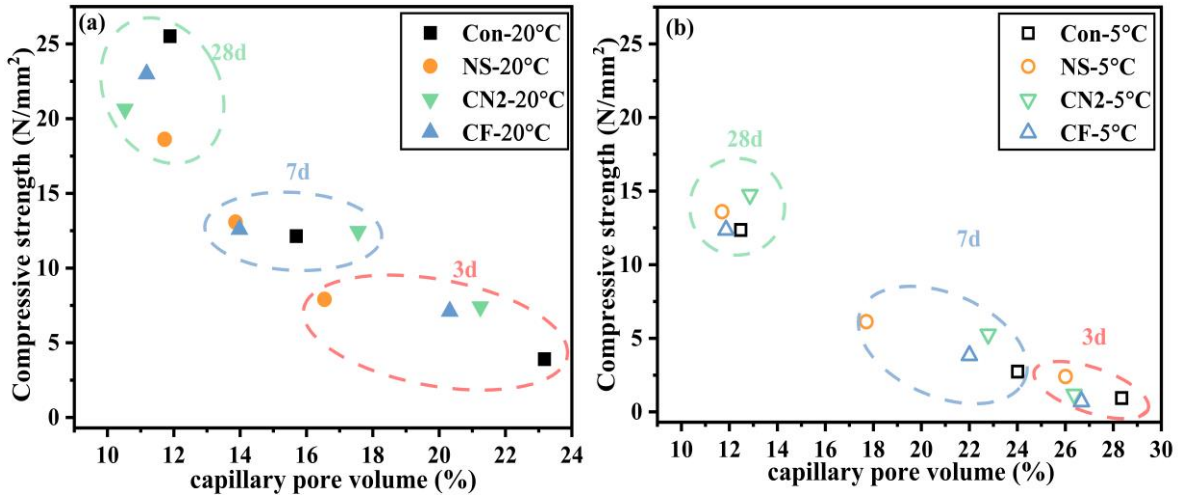

Fig. 6. Temperature plots of compressive strength and capillary porosity: (a) At 20°C and (b) 5 °C.

3.6 Isothermal conduction calorimetry

Figure 7 Shows the calorimetric curves of the pastes cured at 20 and 5 °C. Considering the difference between the temperature set in the instrument and the room temperature, the initial three hours were omitted. Evidently, one exothermic peak of NS could be observed from the heat flow curves of pastes cured at different temperatures, which was earlier and higher than that of the control specimen. The peak occurring at about 12 and 38 h corresponds to the formation of ettringite, which was confirmed by XRD (Fig. S3). The formation of C-A-S-H was related to the broadened peaks of other specimens, which appeared later than NS and control group. This was attributed to the common ionic effect of CF, CN2, and CH, which led to the insufficient dissolution of CH and delayed the hydration of BFS. Comparing the low-temperature curing and room-temperature curing, the trend of cumulative heat curve and heat flow curve was very similar. Comparing the heat flow curve of the two, the appearance of the peak at 5 °C was delayed for about 24 h. This showed that NS could promote the hydration reaction of BFS. Although the exothermic peak appeared later at 5 °C, it could also promote the hydration reaction, which was consistent with the observation results of strength.

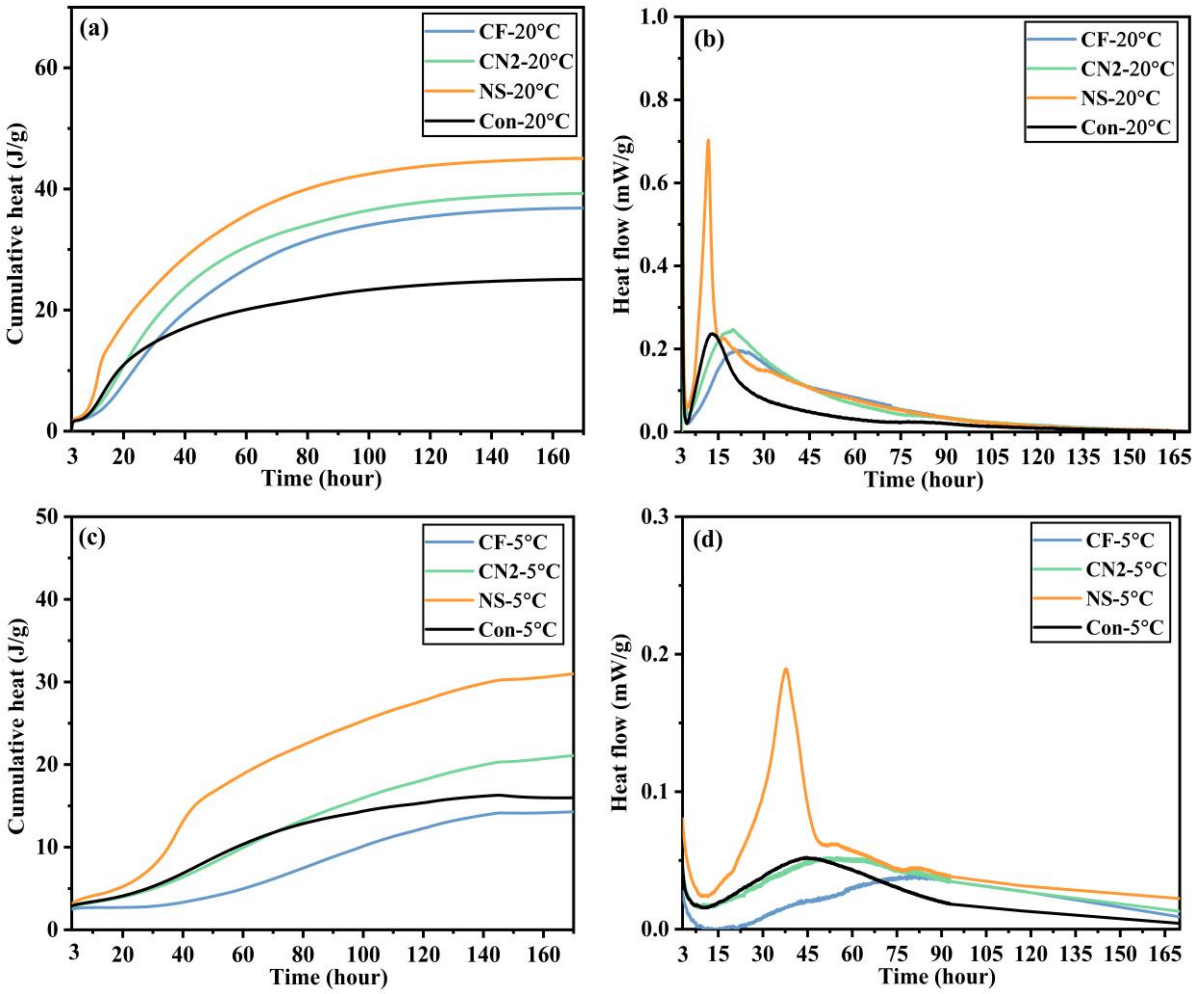

Fig. 7. Calorimetric curves of BFS pastes, (a) cumulative heat cured at 20 °C and (b) heat flow cured at 20 °C, (c) cumulative heat cured at 5 °C, (d) heat flow cured at 5 °C.

3.7 X-ray diffraction (XRD)

Figure 8 shows the XRD patterns of pastes cured at 20 and 5 °C at 28 days. All hydration products, such as monosulfate, hydrotalcite, and ettringite are common products of BFS hydration [40,44,45]. Evidently, low-temperature curing did not change the type of hydration products of the same specimen. Because of the high proportion of calcium hydroxide in the raw materials, carbonization was inevitable, which led to the formation of hemicarbonate aluminate. A wide peak was observed at approximately 28.6°, which may be C-A-S-H. However, because of the poor crystal form of C-A-S-H and overlapping with the peak of slag, this was difficult to distinguish by XRD. The peak of ettringite, which provided early strength, was confirmed by the spectrum of NS. Compared with NS specimens cured at 5 and 20 °C, there was no AFm in the NS spectrum cured at 5 °C. Considering that the formation of AFm mainly followed the dissolution-precipitation mechanism, this showed that the formation of AFm was related to the amount of sulfur and the dissolution rate of sulfur and aluminum. Low temperature delayed the dissolution of slag, resulting in the dissolution rate of aluminum being less than that of sulfur. Even if the amount of NS was small, there was almost no formation of AFm.

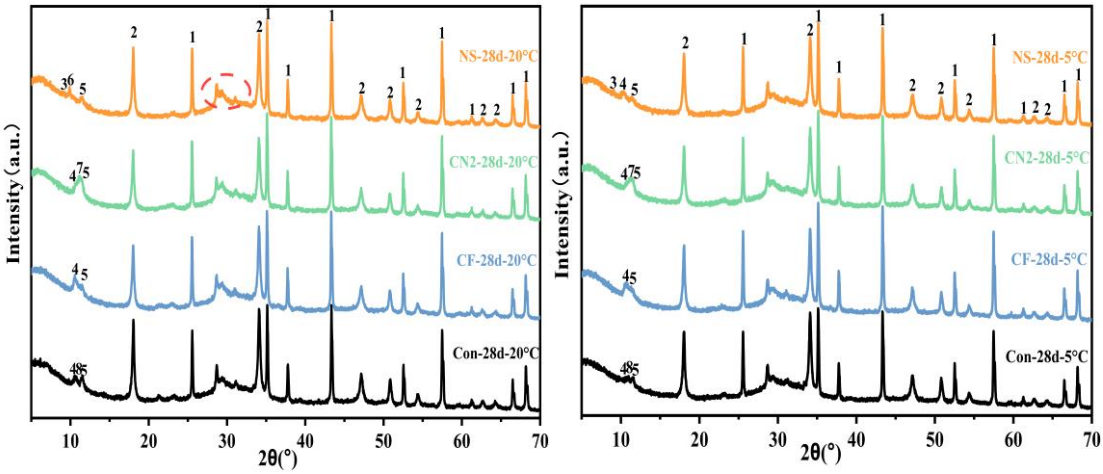

Fig. 8. XRD patterns of pastes cured under different temperatures at 28 day.
(1. α-Al_2O_3 2. Portlandite 3. Ettringite 4. Hemicarbonate 5. Hydrotalcite 6. SO_4-AFm 7. NO_2-AFm 8. C_4AH_{13})

3.8 BSE image analysis

Fig.9 shows a typical example of a backscattered electron image of pastes. According to the different gray levels, the order of brightness from high to low was unreacted slag, portlandite, C-A-S-H, and porosity [46–48].

The hydration degree of the pastes and the relationship between the hydration degree and compressive strength are presented in Fig. 10. Fig. 10(a) shows the hydration degree of the pastes cured at different temperatures. The early hydration degree of all the samples with accelerators cured at 20 °C was higher than that of the control specimen. This indicates that the appropriate dosage of accelerator can promote the hydration of BFS, especially NS, which showed a higher degree of hydration at 3 day. This was also the reason for the higher strength of NS at the early stage. However, from the results of pastes cured at 5 °C, it seems that at low temperatures, except for CN2, other accelerators cannot promote the hydration of slag. Previous studies have shown that the alite reaction is related to the anionic mobility of the additive, and the slag reaction may also be affected by this mechanism [18]. Therefore, the low temperature reduced the ionic activity, resulting in the accelerator not being able to effectively promote the hydration of slag. Fig. 10(b) shows the relationship between the degree of hydration and strength. Generally, the compressive strength increases with an increase in the hydration degree. The trend of the hydration reaction was slightly different from that of the compressive strength.

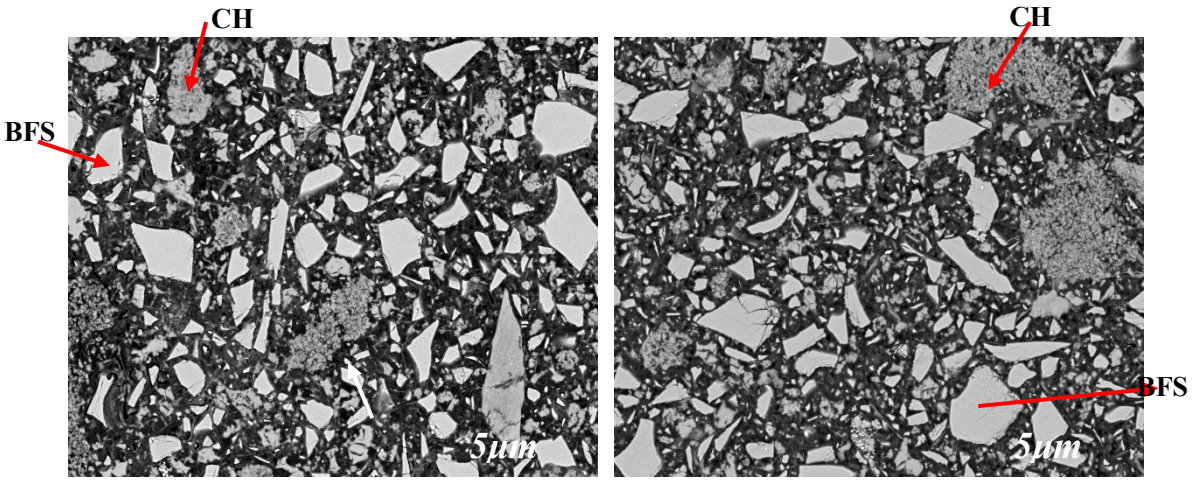

Fig. 9. Backscattered electron image of (a) Con-20 °C and (b) Con-5 °C at 28 day.

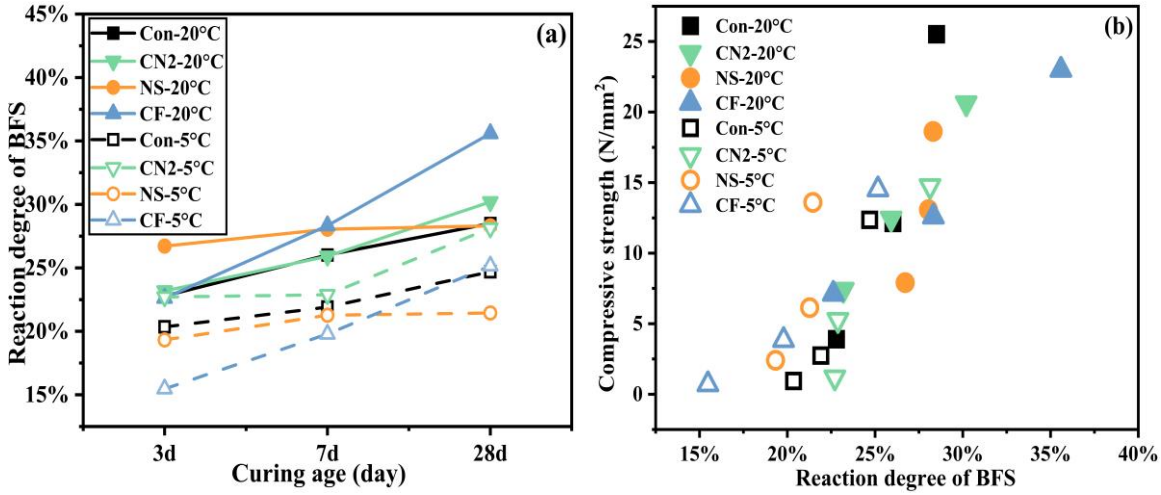

Fig. 10. (a) Reaction degree of BFS and (b) Plot of reaction degree of BFS and compressive strength.

3.9 NMR

The experimental results at 3 day of NMR are shown in Fig. 11. The results on 7 and 28 day are shown in Fig. S4. Because BFS was the only source of Si and Al in this study, the integrated area distributions of ^{27}Al MAS-NMR spectra and ^{29}Si MAS-NMR spectra of all samples were the same. Therefore, all the curves were normalized based on the BFS curve. Fig. 11(a) and (b) show the ^{29}Si MAS-NMR results of the samples cured for 3 days 20 and 5 °C, respectively. As shown in the figure, the peak of unhydrated BFS(Q_0) was ~ 74 ppm [45]. Compared with the control group, the peak of Q_0 of the samples with accelerator added at 3 day under 20 °C decreased more and shifted to a higher ppm value. In particular, the NS showed obvious peaksQ_1 at –78.9 ppm, Q_2(1Al) at –80.9 ppm and Q_2 at –83.7 ppm, which was consistent with the findings of other researchers for alkali-activated BFS [44,45,49,50]. Compared with 20 °C, the peak of all samples at 5 °C almost did not shift, indicating that the degree of hydration was low.

Fig. 11(c) shows the ^{27}Al MAS-NMR results of the samples cured for 3 days at 20 °C. According to a previous study, the peak of C-A-S-H (Al(IV)) was identified at approximately

72 ppm, the broadened peak of unhydrated BFS was identified at 64 ppm, and the peak of pentahedral aluminum was identified at 35 ppm[44,45,50]. The notable area was in the range 2–14 ppm, which marks the distribution area of aluminum octahedral coordinates [45]. The types of AFm produced differed according to the type of additive used. The peak of ettringite (Aft) near 13 ppm and the peak of monosulfate almninate (AFm) and hydrotalcite near 10 ppm were confirmed. A non-assigned peak at 4 ppm was observed in the spectra of all samples, which has also been reported by other researchers [50,51]. This is consistent with the XRD observations. Further, the OH-AFm peak value of CF was significantly stronger than that of the control group, because the only source of aluminum was slag, which indicates that CF promoted the dissolution of slag. Fig. 11(d) shows the ^{27}Al MAS-NMR results of the samples cured for 3 days at 5 °C. It is worth noting that the AFm peak value of CN2 was 17considerably different from that of CF at 20 °C. This may be because the low temperature led to a decrease in ion mobility and a decrease in the dissolution rate of calcium ions under the influence of the common ion effect [42], which limits the hydration of slag. CN2 could promote the hydration of slag because nitrite ions could replace part of the oxyhydrogen ion in AFm.

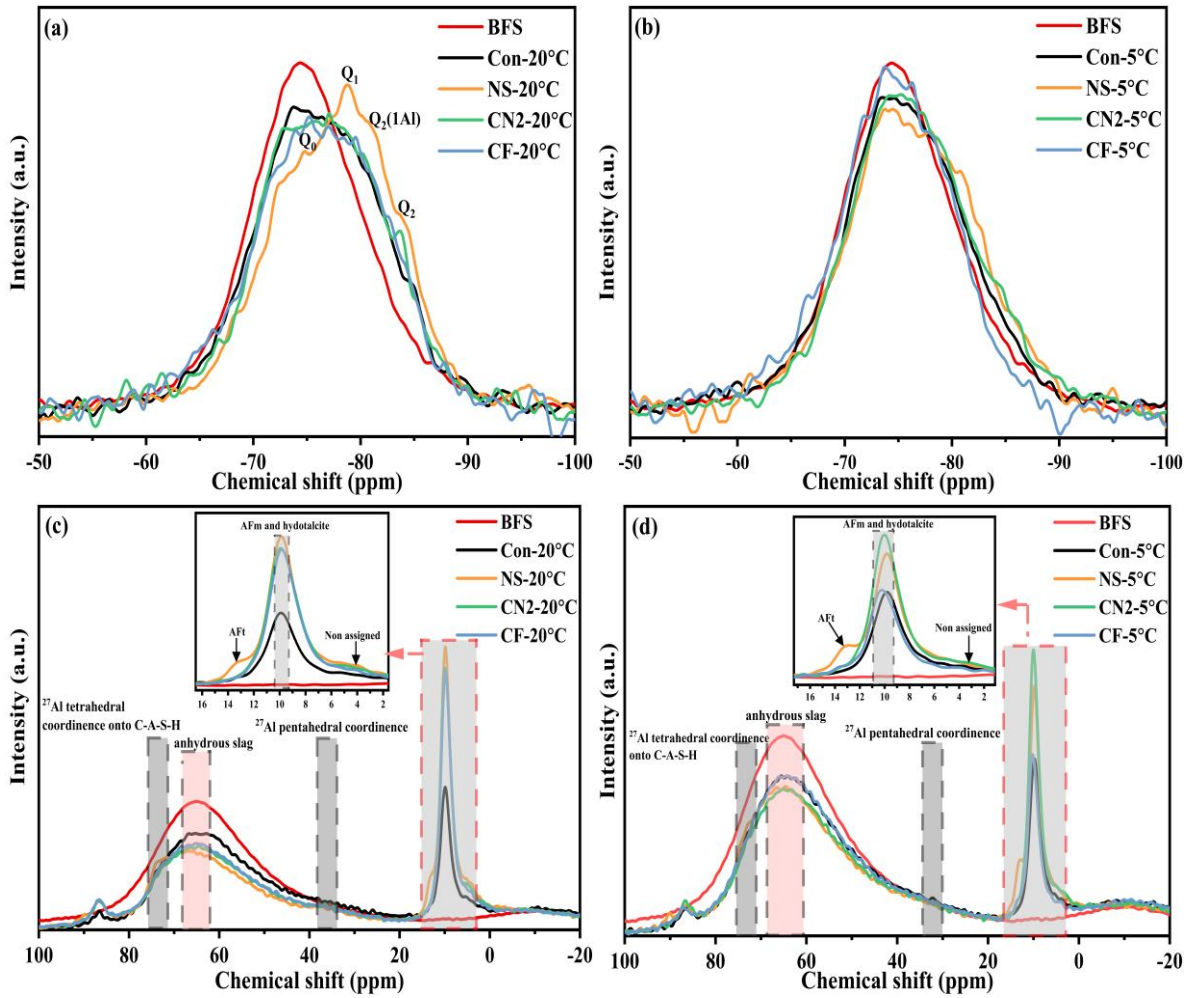

Fig. 11. NMR spectra at of samples cured for 3 days (a) ^{29}Si MAS NMR at 20°C and (b) ^{29}Si MAS NMR at 5°C. (c) ^{27}Al MAS-NMR at 20°C and (d) ^{27}Al MAS-NMR 5°.

3.10 Possible mechanism of accelerator promoting slag hydration

Kondo et al. [18] reported that at an early age of alite, the diffusion rate of anions in the accelerator is faster than that of cations. As the anions penetrate the hydration products on the initial hydrated surface of the alite, it can promote the diffusion of OH^- between the C and A–S–H layers into the liquid phase, increase the pH value of the solution, and promote the hydration of alite. The limiting equivalent ionic conductance (indicating the ionic mobility in solution) was used to characterize the diffusion rate of anions; that is, a larger LEIC indicates a larger diffusion rate, and higher promotion of the hydration of alite. The LEIC values of the anions of the accelerators used in this study and the moles of the corresponding anions are listed in Table 3 [18]. The relationship between the LEIC and compressive strength of the pastes is shown in Fig. 12. A liner correlation was found at 3 days, irrespective of the curing temperature, while a strong negative linear relationship was found at 28 days cured at 20°C. In contrast, However, a weak correlation was observed after 28 days of curing at 5 °C. This indicates that LEIC contributes to the initial strength development, and the strength development mechanism of Alite in the early stage was also applicable to slag. The porosity results (see section 3.3) showed that a coarse pore structure of the samples cured at 5°C at a late stage may inhibit the mobility of ions and decrease the relationship between LEIC and strength.

Table 3 LEIC of accelerators' anions

Ion	LEIC	moles
SO_4^{2-}	79.8	1
NO_2^-	72	2
$HCOO^-$	54.6	2

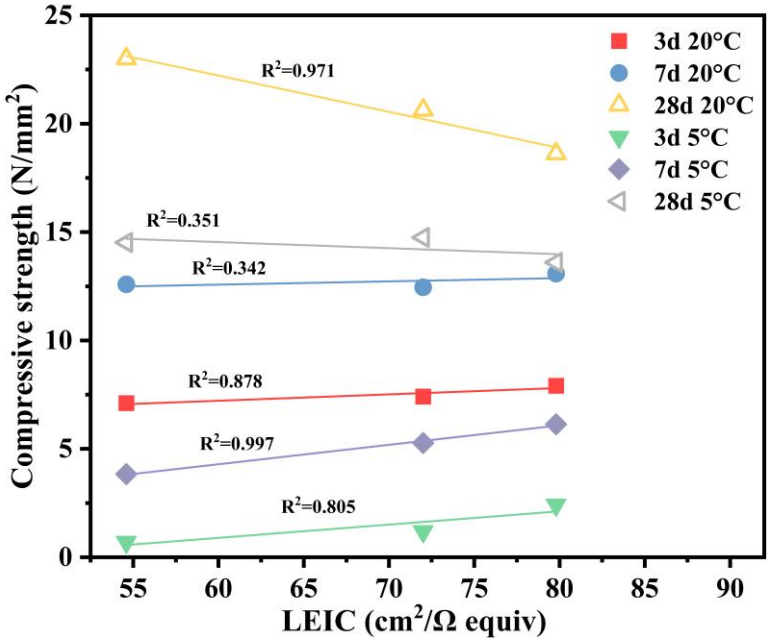

Fig. 12. Relationship between compressive strength and LEIC

The pH value may also affect the hydration of BFS. Before the test, all samples were cured to a specific age (3, 6, and 9 h), and then the pore solution was extracted by centrifugation. A film was used to cover the sample before the measurement to prevent carbonization. A pH meter (HI

99164) was used for this experiment. The change in pH during the first 9 h is shown in Figure 13. According to Fig. 8(b), it can be determined that the slag was in the initial hydrolysis and induction period for the first six hours. According to formula (2), NS can react with calcium hydroxide to form sodium hydroxide (NH) and anhydrate, thus increasing the pH value and promoting the hydrolysis of the Si-O bond in BFS[19]. Therefore, the pH of the NS increased. Fig. 7 (b) shows that NS was the first to complete the induction period. For CF and CN2, it is evident that the values of both are lower than that of the control specimen, which indicates that the formation of hydration products consumes calcium hydroxide and reduces the pH value until the induction stage, reaching a relative equilibrium trend. The change in resistivity on the first day in Fig. 3 (b) can likewise explain this situation. The other reason was that CH accounted for 20 % of the binder in this study. The addition of CF and CN2 increased the concentration of calcium ions. The decomposition of calcium hydroxide was hindered by the common ion effect, resulting in a decrease in the pH value. The order of resistivity from small to large is NS, Con, CF, and CN2, which indicates that NS promotes the hydrolysis of slag and increases the electrolyte of the pore solution.

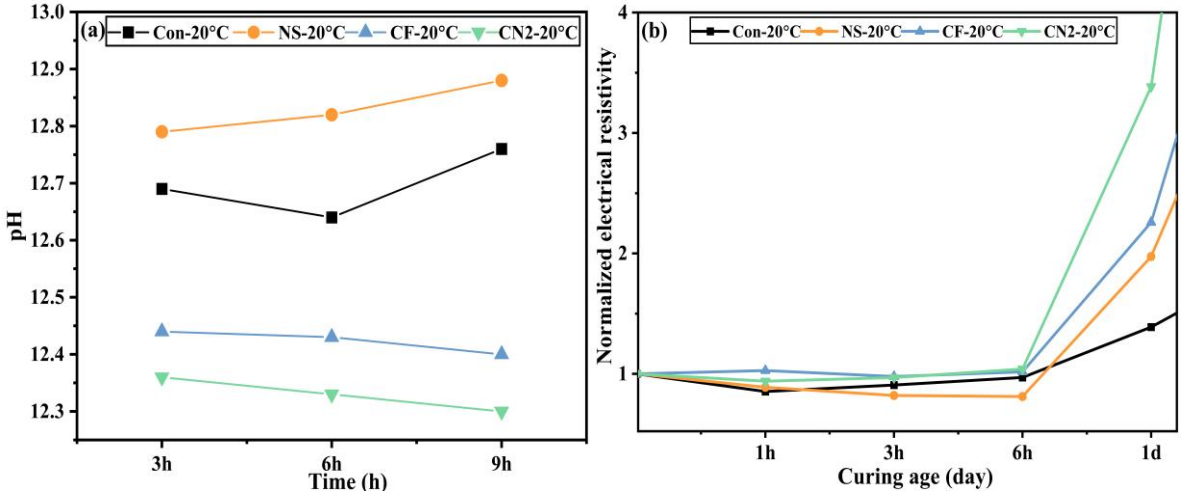

Fig. 13 (a) pH in pore solution and (b) Normalized electrical resistivity on the first day.

To quantitatively predict the relationship between the hydration degree and time of samples with accelerators, the Avrami equation was applied as follows:

$$\alpha = 1 - e^{-a(t-b)^c} \quad (4)$$

where α is the hydration degree of the binder and t is the curing age. The constants a and c were determined by the least-squares method based on the results of BSE. The constant b was set to 0.9, as an empirical value based on previous studies [52]. The calculation results are presented in Table 4. The samples with larger a value demonstrated that the degree of hydration was higher at 3 days, and when c was large, the degree of hydration from 3 to 7 day tended to increase. From the results of NMR, BSE, and compressive strength, the strength development of CN2 and CF was obtained continuously from the early stage.

Table 4
Parameter's calculation results

Sample	a	b	c
Con	0.25 ± 0.02	0.9	0.10 ± 0.02
NS	0.31 ± 0.01		0.03 ± 0.01
CN2	0.24 ± 0.01		0.12 ± 0.01
CF	0.22 ± 0.01		0.21 ± 0.02

4. Conclusions

In this study, the effects and mechanism of accelerators on Ca $(OH)_2$ activated GGBFS cured at 20 and 5°C were investigated by XRD, MIP, NMR, isothermal conduction calorimetry, and SEM. The main results are as follows:

(1) Accelerators can still promote the strength development of pastes in the early stage under low-temperature curing, especially NS, which shows higher strength and hydration degree in the early stage of hydration; however, this also becomes one of the reasons why the strength of NS is weaker than that of other samples in the later stage.

(2) At low temperatures, the accelerators can reduce the porosity of the samples to a certain extent, but compared to 20 °C, the pore size distribution of the sample was poor, and the porosity was high, which is one of the main problems of low-temperature curing. In addition, the accelerators cannot effectively improve the pore structure during low-temperature curing, which seriously restricts the development of strength.

(3) The results of XRD and isothermal calorimetry showed that the exothermic curves of the samples at 5 and 20 °C were very similar. It was confirmed by XRD that low-temperature curing did not change the hydration products. Because of the slow hydration at low temperature, it is difficult to observe the exothermic peak, except NS, which is mainly due to the increase in sulfate ion content and the formation of ettringite in the early stage. This may also be one of the reasons for the high strength of the NS samples at an early stage.

(4) NMR results show that at low temperatures, owing to the influence of low ionic mobility and common ion effect, CF leads to a decrease in the solubility of Ca $(OH)_2$, which hinders the hydration of BFS at an early age. Although CN2 has the same problem, nitrite ions can replace part of the hydroxyl ion in the AFm intermediate layer, so the promoting effect is larger than the inhibition effect.

(5) A liner correlation was found between the LEIC and compressive strength of the pastes curing at 3 days, irrespective of the curing temperature and a strong negative linear correlation was found at 28 days cured at 20°C, while a weak correlation was found at 5 °C. This suggests that LEIC influences the reaction acceleration of blast-furnace slag at an early age, whereas the coarse pore structure of the samples cured at 5°C at late stage reduces the correlation between LEIC and strength.

Acknowledgement

This work was supported by JSPS KAKENHI Grant Number 21K04349 and the Steel Foundation for Environmental Protection Technology.

References

[1] H.F.W. Taylor, Cement chemistry, 1997. https://doi.org/10.1680/cc.25929.

[2] M.M.A. Elahi, C.R. Shearer, A. Naser Rashid Reza, A.K. Saha, M.N.N. Khan, M.M. Hossain, P.K. Sarker, Improving the sulfate attack resistance of concrete by using supplementary cementitious materials (SCMs): A review, Constr. Build. Mater. 281 (2021). https://doi.org/10.1016/j.conbuildmat.2021.122628.

[3] S. Ramanathan, M. Croly, P. Suraneni, Comparison of the effects that supplementary cementitious materials replacement levels have on cementitious paste properties, Cem. Concr. Compos. 112 (2020). https://doi.org/10.1016/j.cemconcomp.2020.103678.

[4] L.A. Qureshi, B. Ali, A. Ali, Combined effects of supplementary cementitious materials (silica fume, GGBS, fly ash and rice husk ash) and steel fiber on the hardened properties of recycled aggregate concrete, Constr. Build. Mater. 263 (2020). https://doi.org/10.1016/j.conbuildmat.2020.120636.

[5] G. Jing, Z. Ye, J. Wu, S. Wang, X. Cheng, V. Strokova, V. Nelyubova, Introducing reduced graphene oxide to enhance the thermal properties of cement composites, Cem. Concr. Compos. 109 (2020). https://doi.org/10.1016/j.cemconcomp.2020.103559.

[6] W. Baomin, D. Shuang, Effect and mechanism of graphene nanoplatelets on hydration reaction, mechanical properties and microstructure of cement composites, Constr. Build. Mater. 228 (2019). https://doi.org/10.1016/j.conbuildmat.2019.116720.

[7] E. Horszczaruk, Properties of cement-based composites modified with magnetite nanoparticles: A review, Materials (Basel). 12 (2019). https://doi.org/10.3390/ma12020326.

[8] F. Bellmann, J. Stark, Activation of blast furnace slag by a new method, Cem. Concr. Res. 39 (2009). https://doi.org/10.1016/j.cemconres.2009.05.012.

[9] R.A. Rivera, M.Á. Sanjuán, D.A. Martín, Granulated blast-furnace slag and coal fly ash ternary portland cements optimization, Sustain. 12 (2020). https://doi.org/10.3390/su12145783.

[10] J. Liu, Q. Yu, Z. Zuo, F. Yang, Z. Han, Q. Qin, Reactivity and performance of dry granulation blast furnace slag cement, Cem. Concr. Compos. 95 (2019). https://doi.org/10.1016/j.cemconcomp.2018.10.008.

[11] L. Ben-Dor, D. Perez, Influence of admixtures on strength development of Portland cement and on the microstructure of tricalcium silicate, J. Mater. Sci. 11 (1976) 239–245. https://doi.org/10.1007/BF00551433.

[12] R. Kondo, C.T. Song, S. Goto, M. Daimon, Latent Hydraulic Property of Granulated Blast Furnace Slag By Various Activators., Tetsu-To-Hagane/Journal Iron Steel Inst. Japan. 65 (1979) 1825–1829. https://doi.org/10.2355/tetsutohagane1955.65.13_1825.

[13] T. Vehmas, A. Kronlöf, A. Cwirzen, Calcium chloride acceleration in ordinary Portland cement, Mag. Concr. Res. 70 (2018) 856–863. https://doi.org/10.1680/jmacr.17.00079.

[14] R. Myrdal, SINTEF REPORT: Advanced cementing materials - Controlling hydration development - Accelerating admixtures for concrete - State of the art, 2007. www.sintef.no/coin.

[15] Y. Tao, A.V. Rahul, K. Lesage, Y. Yuan, K. Van Tittelboom, G. De Schutter, Stiffening control of cement-based materials using accelerators in inline mixing processes:

Possibilities and challenges, Cem. Concr. Compos. 119 (2021) 103972. https://doi.org/10.1016/j.cemconcomp.2021.103972.
[16] S. Aggoun, M. Cheikh-Zouaoui, N. Chikh, R. Duval, Effect of some admixtures on the setting time and strength evolution of cement pastes at early ages, Constr. Build. Mater. 22 (2008) 106–110. https://doi.org/10.1016/j.conbuildmat.2006.05.043.
[17] K. Riding, D.A. Silva, K. Scrivener, Early age strength enhancement of blended cement systems by CaCl2 and diethanol-isopropanolamine, Cem. Concr. Res. 40 (2010) 935–946. https://doi.org/10.1016/j.cemconres.2010.01.008.
[18] R. Kondo, M. Daimon, E. Sakai, H. Ushiyama, Influence of inorganic salts on the hydration of tricalcium silicate, J. Biochem. Toxicol. 27 (1977) 191–197. https://doi.org/10.1002/jbt.2570270128.
[19] J. Fu, A.M. Jones, M.W. Bligh, C. Holt, L.M. Keyte, F. Moghaddam, S.J. Foster, T.D. Waite, Mechanisms of enhancement in early hydration by sodium sulfate in a slag-cement blend – Insights from pore solution chemistry, Cem. Concr. Res. 135 (2020) 106110. https://doi.org/10.1016/j.cemconres.2020.106110.
[20] Y. Li, H. Sun, X. Liu, Z. Cui, Effect of phase separation structure on cementitious reactivity of blast furnace slag, Sci. China, Ser. E Technol. Sci. 52 (2009). https://doi.org/10.1007/s11431-008-0239-x.
[21] J.M. Richardson, J.J. Biernacki, P.E. Stutzman, D.P. Bentz, Stoichiometry of slag hydration with calcium hydroxide, J. Am. Ceram. Soc. 85 (2002) 947–953. https://doi.org/10.1111/j.1151-2916.2002.tb00197.x.
[22] J.J. Biernacki, J.M. Richardson, P.E. Stutzman, D.P. Bentz, Kinetics of slag hydration in the presence of calcium hydroxide, J. Am. Ceram. Soc. 85 (2002) 2261–2267. https://doi.org/10.1111/j.1151-2916.2002.tb00445.x.
[23] M. Ojima, K. Sasaki, K. Kurumisawa, Effect of accelerating admixture on early strength development of blast-furnace slag cement paste, Cem. Sci. Concr. Technol. 72 (2019). https://doi.org/10.14250/cement.72.114.
[24] Y. Yamada, K. Kurumisawa, Improvement of initial strength of blast furnace slag cement paste using frost damage inhibitor by accelerator, Cem. Sci. Concr. Technol. 73 (2020). https://doi.org/10.14250/cement.73.103.
[25] K. Federowicz, V.A. Figueiredo, H. Al-Kroom, H.A. Abdel-Gawwad, M.A. Elrahman, P. Sikora, The effects of temperature curing on the strength development, transport properties, and freeze-thaw resistance of blast furnace slag cement mortars modified with nanosilica, Materials (Basel). 13 (2020). https://doi.org/10.3390/ma13245800.
[26] T. Medina-Serna, S. Arredondo-Rea, J. Gómez-Soberón, C. Rosas-Casarez, R. Corral-Higuera, Effect of curing temperature in the alkali-activated blast-furnace slag paste and their structural influence of porosity, Adv. Sci. Technol. Res. J. 10 (2016). https://doi.org/10.12913/22998624/64021.
[27] T. Bakharev, J.G. Sanjayan, Y.B. Cheng, Effect of elevated temperature curing on properties of alkali-activated slag concrete, Cem. Concr. Res. 29 (1999). https://doi.org/10.1016/S0008-8846(99)00143-X.
[28] M. Soutsos, F. Kanavaris, M. Elsageer, Accuracy of maturity functions' strength estimates for fly ash concretes cured at elevated temperatures, Constr. Build. Mater. 266 (2021). https://doi.org/10.1016/j.conbuildmat.2020.121043.

[29] L.S. Ho, K. Nakarai, M. Duc, A. Le Kouby, A. Maachi, T. Sasaki, Analysis of strength development in cement-treated soils under different curing conditions through microstructural and chemical investigations, Constr. Build. Mater. 166 (2018). https://doi.org/10.1016/j.conbuildmat.2018.01.112.
[30] S.F.A. Shah, B. Chen, S.Y. Oderji, M.A. Haque, M.R. Ahmad, Improvement of early strength of fly ash-slag based one-part alkali activated mortar, Constr. Build. Mater. 246 (2020). https://doi.org/10.1016/j.conbuildmat.2020.118533.
[31] Z. Liu, B. Lou, D.M. Barbieri, A. Sha, T. Ye, Y. Li, Effects of pre-curing treatment and chemical accelerators on Portland cement mortars at low temperature (5 °C), Constr. Build. Mater. 240 (2020). https://doi.org/10.1016/j.conbuildmat.2019.117893.
[32] D.P. Bentz, P.E. Stutzman, F. Zunino, Low-temperature curing strength enhancement in cement-based materials containing limestone powder, Mater. Struct. Constr. 50 (2017). https://doi.org/10.1617/s11527-017-1042-6.
[33] X. Wei, D. Li, F. Ming, C. Yang, L. Chen, Y. Liu, Influence of low-temperature curing on the mechanical strength, hydration process, and microstructure of alkali-activated fly ash and ground granulated blast furnace slag mortar, Constr. Build. Mater. 269 (2021). https://doi.org/10.1016/j.conbuildmat.2020.121811.
[34] A Practical Guide to Microstructural Analysis of Cementitious Materials, 2018. https://doi.org/10.1201/b19074.
[35] P.A. Bingham, A.J. Connelly, R.J. Hand, N.C. Hyatt, P.A. Northrup, R. Alonso Mori, P. Glatzel, M. Kavčič, M. Žitnik, K. Bučar, R. Edge, A multi-spectroscopic investigation of sulphur speciation in silicate glasses and slags, Glas. Technol. Eur. J. Glas. Sci. Technol. Part A. 51 (2010).
[36] S.A. BernaL, X. Ke, O.H. Hussein, J.L. Provis, Effect of testing conditions on the loss on ignition results of anhydrous granulated blast furnace slags determined via thermogravimetry, in: Int. RILEM Conf. Mater. Syst. Struct. Civ. Eng. Conf. Segm. Concr. with Suppl. Cem. Mater., 2016.
[37] K. Tanaka, K. Kurumisawa, Development of technique for observing pores in hardened cement paste, Cem. Concr. Res. 32 (2002). https://doi.org/10.1016/S0008-8846(02)00806-2.
[38] K. Kurumisawa, Effect of inorganic salts on reaction of blast furnace slag composite, C. Science, C. Technology, 1. 2. 2. 1, 74 (n.d.) 105–110.
[39] B. Mota, T. Matschei, K. Scrivener, Impact of NaOH and Na2SO4 on the kinetics and microstructural development of white cement hydration, Cem. Concr. Res. 108 (2018). https://doi.org/10.1016/j.cemconres.2018.03.017.
[40] Y. Zhao, J. Gao, Z. Xu, S. Li, X. Luo, G. Chen, Long-term hydration and microstructure evolution of blended cement containing ground granulated blast furnace slag and waste clay brick, Cem. Concr. Compos. 118 (2021). https://doi.org/10.1016/j.cemconcomp.2021.103982.
[41] P. Pipilikaki, M. Beazi-Katsioti, The assessment of porosity and pore size distribution of limestone Portland cement pastes, Constr. Build. Mater. 23 (2009). https://doi.org/10.1016/j.conbuildmat.2008.08.028.
[42] W.S. Yum, J. Il Suh, S. Sim, S. Yoon, Y. Jun, J.E. Oh, Influence of calcium and sodium nitrate on the strength and reaction products of the CaO-activated GGBFS system, Constr.

Build. Mater. 215 (2019). https://doi.org/10.1016/j.conbuildmat.2019.04.240.
[43] L. Zhang, J. Zhou, Fractal characteristics of pore structure of hardened cement paste prepared by pressurized compact molding, Constr. Build. Mater. 259 (2020). https://doi.org/10.1016/j.conbuildmat.2020.119856.
[44] J. Schneider, M.A. Cincotto, H. Panepucci, 29Si and 27Al high-resolution NMR characterization of calcium silicate hydrate phases in activated blast-furnace slag pastes, Cem. Concr. Res. 31 (2001). https://doi.org/10.1016/S0008-8846(01)00530-0.
[45] Y. Jeong, J.E. Oh, Y. Jun, J. Park, J.H. Ha, S.G. Sohn, Influence of four additional activators on hydrated-lime [Ca(OH)2] activated ground granulated blast-furnace slag, Cem. Concr. Compos. 65 (2016). https://doi.org/10.1016/j.cemconcomp.2015.10.007.
[46] V. Kocaba, E. Gallucci, K.L. Scrivener, Methods for determination of degree of reaction of slag in blended cement pastes, Cem. Concr. Res. 42 (2012). https://doi.org/10.1016/j.cemconres.2011.11.010.
[47] B.S. Gebregziabiher, R. Thomas, S. Peethamparan, Very early-age reaction kinetics and microstructural development in alkali-activated slag, Cem. Concr. Compos. 55 (2015). https://doi.org/10.1016/j.cemconcomp.2014.09.001.
[48] S.D. Wang, K.L. Scrivener, Hydration products of alkali activated slag cement, Cem. Concr. Res. 25 (1995). https://doi.org/10.1016/0008-8846(95)00045-E.
[49] M. Palacios, F. Puertas, Effect of carbonation on alkali-activated slag paste, J. Am. Ceram. Soc. 89 (2006). https://doi.org/10.1111/j.1551-2916.2006.01214.x.
[50] S. Murgier, H. Zanni, D. Gouvenot, Blast furnace slag cement: A 29Si and 27Al NMR study, Comptes Rendus Chim. 7 (2004). https://doi.org/10.1016/j.crci.2004.02.004.
[51] M. Saillio, V. Baroghel-Bouny, S. Pradelle, M. Bertin, J. Vincent, J.B. d'Espinose de Lacaillerie, Effect of supplementary cementitious materials on carbonation of cement pastes, Cem. Concr. Res. 142 (2021). https://doi.org/10.1016/j.cemconres.2021.106358.
[52] H.F.W. Taylor, A method for predicting alkali ion concentrations in cement pore solutions, Adv. Cem. Res. 1 (1987). https://doi.org/10.1680/adcr.1987.1.1.5.